Title
Breast tissue decomposition with spectral distortion correction: A postmortem study

Journal
Medical Physics, 41(10)

ISSN
0094-2405

Authors
Ding, Huanjun
Zhao, Bo
Baturin, Pavlo
et al.

Publication Date
2014-09-12

DOI
10.1118/1.4894724

Breast tissue decomposition with spectral distortion correction: A postmortem study

Huanjun Ding, Bo Zhao, Pavlo Baturin, Farnaz Behroozi, and Sabee Molloi[a)]
Department of Radiological Sciences, University of California, Irvine, California 92697

(Received 14 April 2014; revised 11 July 2014; accepted for publication 20 August 2014; published 12 September 2014)

Purpose: To investigate the feasibility of an accurate measurement of water, lipid, and protein composition of breast tissue using a photon-counting spectral computed tomography (CT) with spectral distortion corrections.
Methods: Thirty-eight postmortem breasts were imaged with a cadmium-zinc-telluride-based photon-counting spectral CT system at 100 kV. The energy-resolving capability of the photon-counting detector was used to separate photons into low and high energy bins with a splitting energy of 42 keV. The estimated mean glandular dose for each breast ranged from 1.8 to 2.2 mGy. Two spectral distortion correction techniques were implemented, respectively, on the raw images to correct the nonlinear detector response due to pulse pileup and charge-sharing artifacts. Dual energy decomposition was then used to characterize each breast in terms of water, lipid, and protein content. In the meantime, the breasts were chemically decomposed into their respective water, lipid, and protein components to provide a gold standard for comparison with dual energy decomposition results.
Results: The accuracy of the tissue compositional measurement with spectral CT was determined by comparing to the reference standard from chemical analysis. The averaged root-mean-square error in percentage composition was reduced from 15.5% to 2.8% after spectral distortion corrections.
Conclusions: The results indicate that spectral CT can be used to quantify the water, lipid, and protein content in breast tissue. The accuracy of the compositional analysis depends on the applied spectral distortion correction technique. © *2014 American Association of Physicists in Medicine.* [http://dx.doi.org/10.1118/1.4894724]

Key words: spectral CT, breast tissue decomposition, spectral distortion correction

1. INTRODUCTION

Currently, mammography is the standard imaging modality for breast cancer screening.[1] However, the sensitivity and specificity of this technique are limited due to the overlap of breast parenchyma, especially for dense breasts.[2–4] To address these limitations, dedicated breast computed tomography (CT) systems, which scan in the coronal plane around the breast in its pendant geometry, have been recently investigated.[5–14] This technique has been reported to have improved sensitivity due to its ability to provide 3D information. In addition, breast CT offers the opportunity to characterize suspicious lesions according to its composition with spectral imaging.[15,16]

A recent report suggests that, in addition to irregular mass shape, speculated mass margin, and patient age, an increase in mammographic attenuation of a mass also increases its likelihood of malignancy.[17] However, high mass density by itself is not sufficiently accurate to avert the need for a biopsy. If lesions could be characterized quantitatively according to their chemical compositions, predictive capability might be improved. Thus, there is increased interest in developing lesion characterization techniques that can accurately quantify the chemical components in suspicious lesions. Both malignant and benign lesions are expected to have higher water content than normal breast tissue since the increased cell water content not only promotes cell division and oncogene expression, but also accelerates cells' respiration rate, which enhances their ability to compete for nutrients with normal cells.[18] Previous reports using diffuse optical spectroscopy have suggested that malignant tumors have reduced lipid (~20%) and increased water (>50%) contents compared to normal breast tissue.[19–22] In addition, other reports suggest a positive correlation between increased tissue water content and carcinogenesis.[23] Although the water content in benign lesions may vary significantly depending on the type of lesions,[24] the quantitative information of lesion composition can be used to improve the positive predictive value for cancer detection. A recent clinical study has suggested that knowledge of the breast lesion composition may improve the distinction between different benign and malignant lesion types in dual energy mammography.[25]

However, the three-compartment characterization of a lesion can be challenging with the current x-ray imaging technology. Unlike calcification or iodinated contrast agent, the x-ray attenuation properties of water, lipid, and protein have small differences in the diagnostic energy range.[26] Decomposition noise induced by image misregistration or spectral overlapping may easily reduce the signal-to-noise ratio (SNR) to the level where no reliable measurement can be obtained. The recent development of photon-counting x-ray detectors capable of counting individual photons and sorting them by energy

offers unique advantages in tissue characterization.[15,27–29] A proper selection of the energy threshold can minimize the spectral overlap and allow simultaneous acquisition of the dual energy images within a single scan, which eliminates the risks of misregistration.

State of the art photon-counting detectors based on semiconductors such as silicon,[30–34] cadmium telluride (CdTe)[27,35–38] and cadmium-zinc-telluride (CZT)[29,39–41] offer a maximum count rate over 10^7 (counts/s)/mm^2.[42–44] However, the detector response may become nonlinear under such high count rates due to various artifacts such as pulse pileup, characteristic escape, and charge-sharing.[45–48] Spectral CT imaging depends critically on a reliable measure of the energy-dependent attenuation coefficients for different materials. The presence of nonlinear detector response leads to substantial distortions in the recorded spectral information, which can severely limit the detector's energy discriminating capability. A recent report has suggested that at high count rates, the benefit of using photon-counting detectors is diminished due to spectrum distortion.[49] Thus, it is critical to develop a technique that will account for the distortions in the output spectrum so reliable measurements can be made at the desired flux.

Spectral distortion in photon-counting detectors can be attributed to several artifacts which are associated with both charge generation and transport in semiconductor crystals and pulse height analysis in readout electronics. The development of the hardware-based correction techniques may remain challenging in the near future. Furthermore, due to the complex nature of the problem, it will also be difficult to provide a correction algorithm based on analytical simulations. In previous studies, an image-based semiempirical spectral distortion correction method has been proposed.[50] In a phantom study, the method can effectively reduce decomposition errors caused by spectral distortion. Furthermore, rather than detector-specific simulation packages, the method requires a relatively simple calibration process and knowledge about the incident spectrum.[50] The purpose of this study was to further validate the image-based spectral distortion correction method with a postmortem study. Here, we investigated the feasibility of tissue decomposition of postmortem breasts, in terms of water, lipid, and protein content, with a spectral CT system based on a CZT photon-counting detector. The recorded dual energy images were processed with two spectral distortion correction methods. The dual energy decomposition measurement of the tissue compositions was compared to the reference standard obtained from definitive tissue chemical analysis. The accuracy of dual energy decomposition was compared between the raw and the distortion-corrected data sets.

2. MATERIALS AND METHODS

2.A. Photon-counting spectral CT system

A bench-top spectral CT system used in this study is shown in Fig. 1. The system consisted of a tungsten target x-ray tube (Dynamax 78E) coupled with a Phillips Optimus M200 x-ray generator and filtered with 2 mm Al and 0.15 mm Cu, fore and aft collimators made of 3 mm thick lead sheets with 0.3 and 0.8 mm slit widths, respectively. A high precision motor (Kollmorgen Goldline DDR D062M, Danaher Motion, Wood Dale, IL) served as the rotational sample platform. A CZT-based photon-counting detector (eV2500, eV Microelectronics Inc., Saxonburg, PA) consisting of a linear row of four CZT crystals with 12.8 mm in length, 3 mm in width, and 3 mm in thickness. Each crystal consisted of 16 pixels, yielding a total of 64 pixels with an effective pixel pitch of 0.8 mm. The entrance beam to the detector was shaped by a brass collimator and collimated the height of each pixel to 0.8 mm. A field programmable gate array (FPGA) chip was used to count the trigger pulses generated by five comparators from each pixel over a user defined collection period, selectable from 1 to 50 ms. Each frame was sent to a workstation over a USB interface for data processing, storage, and visualization. The acquired photons were sorted into five user-definable energy bins and the energy resolution was calibrated up to 140 keV by the manufacturer of the detector (Endicott Interconnect Detection and Imaging Systems). The linear count rate range derived from a thickness-dependent study was 1.2×10^6 (counts/s)/mm^2. The detector itself did not have any pulse pileup and charge-sharing correction mechanisms.

A bias voltage of 1000 V was placed across the CZT crystal and the detector was operated in Ohmic mode. An electron hole pair was created as a photon interacted with the CZT crystal and transferred energy above 4.64 eV to the crystal. The generated electrons were collected at the back electrode and then formed a pulse whose height was proportional to the energy of the absorbed photon by the ASIC. If the pulse height was higher than the given threshold value, a count was registered. The lower boundaries of the energy bins were defined by five user-definable thresholds, therefore, the count within an energy bin could be easily obtained by subtracting the count from its two adjacent thresholds. The count difference between the two thresholds provided the number of recorded counts as a function of energy.

The source-to-detector distance (SID) and the source-to-object distance (SOD) were 1.33 and 0.93 m, respectively, leading to a magnification of 1.4. To address the detector size limitation, a translation stage controlled by two-step motors was used to move the sample stage in both vertical and horizontal directions. The overall field of view (FOV) in the fan beam plane could thus be expanded up to 12 cm at the isocenter by stitching four scans together.

2.B. Calibration phantom and postmortem breast samples

A cylindrical calibration phantom with a diameter of 3.2 cm was constructed from polymethylene plastic (Delrin, Mac Master Carr, Inc., Elmhurst, IL), which has been shown previously to be a good candidate for representing the x-ray attenuation properties of protein.[16,51] Two holes, with a diameter of 0.95 cm, were drilled in the phantom and were subsequently filled with water and vegetable oil. Thus, the three-compartment phantom consisted of surrogate materials

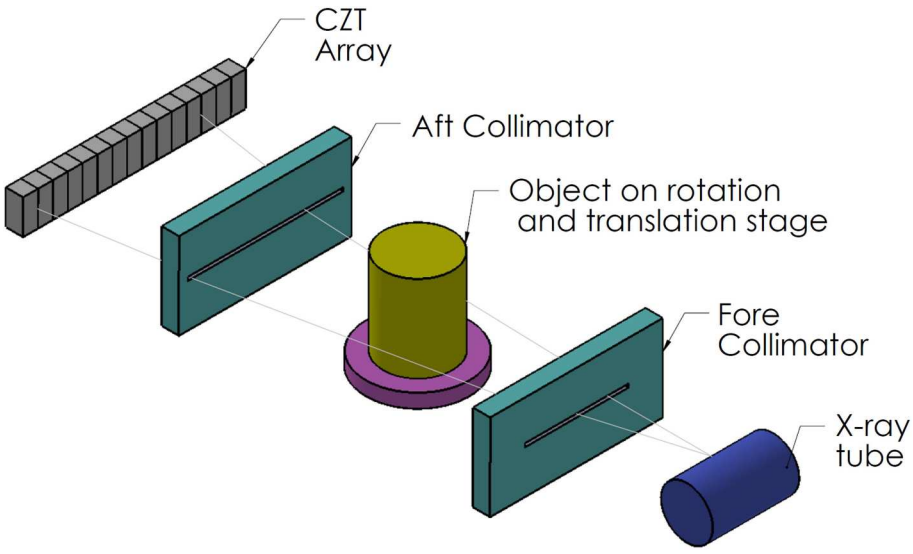

FIG. 1. A sketch of the bench-top photon-counting spectral CT system.

for water, lipid, and protein, in terms of their x-ray attenuation properties, respectively. The justification and the potential errors induced by the calibration material selection have been previously reported.[16,26]

Twenty pairs (left and right) of postmortem breasts were acquired from the Willed Body Program in the School of Medicine at University of California, Irvine. The breasts, including skin, were surgically removed from the cadaver to the pectoralis major muscle and kept frozen inside labeled plastic bags. The mass of the breasts varied from 136 to 2330 g. The breast density, as estimated from cone-beam CT scans, was approximately in the range of 5%–70%. The breasts were removed from the freezer and kept at approximately 4 °C for a day before the experiment. To prevent any water loss during the experiment, the breasts were wrapped with a thin, very low attenuating, plastic film (GLAD cling wrap, The Glad Production Co., Oakland, CA), and shaped into cylinders with a diameter of approximately 10 cm using white polystyrene foam which is almost transparent to x-ray. Before each CT scan, samples were kept at room temperature for at least 30 min to allow for tissue relaxation.

2.C. Dual energy image acquisition and processing

The CZT detector was used to generate dual energy images during a single scan by separating the low and high energy bins with a splitting energy. According to a previous simulation study,[15] the optimal imaging protocols, in terms of the tube voltage and the splitting energy for water, lipid, and protein decomposition were selected to be 100 kV(peak) and 42 keV in the current postmortem study, respectively. The measured open field x-ray spectrum is shown in Fig. 2 with the selection of the splitting energy. The mean glandular dose (MGD) for a 14 cm breast of 30% glandularity, is approximately 2.0 mGy according to previous Monte Carlo simulations.[52] A flat-field calibration was applied to correct the pixel nonuniformity, using an open source image processing software package.[53] The sample stage rotated at a speed of approximately 0.976 rpm during image acquisition. The detector frame rate was set at 20 frames/s. Therefore, a total of 1229 frames were acquired for 360° rotation where each frame covered approximately 0.3°. Helical scans with pitch of two were performed to cover the 3D volume of the breasts. Limited by the detector FOV, each helical scan only covered part of the sample volume. The scanning stage was used to extend the FOV. Four helical scans were performed on each sample; the resulting sinograms were stitched together to cover the whole breast before filtered back-projection (FBP) reconstruction. The voxel values in the reconstructed dual energy CT images were represented by the effective attenuation coefficients for the corresponding energy bins, which were used for dual energy decomposition.[15]

Three-material decomposition was achieved with an additional constraint, which assumed that the total volume of

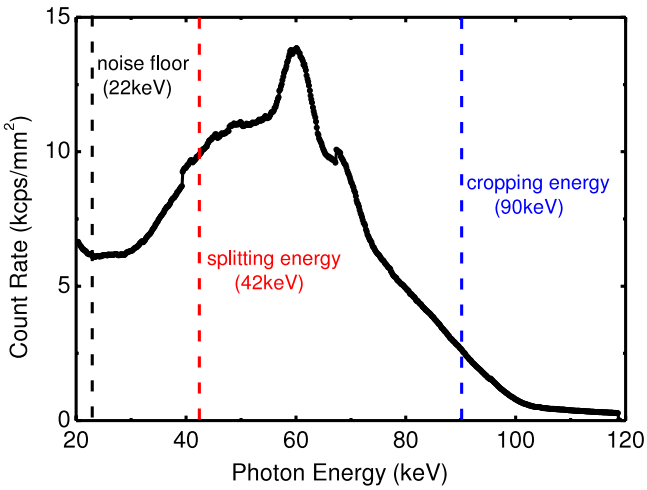

FIG. 2. The experimentally measured tungsten anode spectrum at 100 kV(peak) before attenuated by the breast. The electronic noise floor, the splitting threshold between low and high energy bins, and the cropping energy used to reject pulse pileup were noted as dashed lines at 22, 42, and 90 keV, respectively.

water, lipid, and protein in each voxel equals the known voxel size. The tissue compositions can then be calculated based on the measured linear attenuation[26]

$$\begin{pmatrix} \mu_W^L & \mu_L^L & \mu_P^L \\ \mu_W^H & \mu_L^H & \mu_P^H \\ 1 & 1 & 1 \end{pmatrix} \begin{pmatrix} f_W \\ f_L \\ f_P \end{pmatrix} = \begin{pmatrix} U^L \\ U^H \\ 1 \end{pmatrix}, \quad (1)$$

where μ_W^L, μ_L^L and μ_P^L are the linear attenuation coefficients of water, lipid, and protein, respectively. f_W, f_L, and f_P represent the volume fractions of water, lipid, and protein, respectively. U^L and U^H are the measured attenuations of the images from the low and the high energy bins, respectively.

A linear calibration function [Eq. (2)] was used to solve for f_W, f_L and f_P in a two-step process. A calibration phantom was first imaged to determine the system calibration coefficients (a_0, a_1, and a_2) by least-squares fitting.[15] Then, the dual energy signals of the postmortem breasts were measured for the entire volumes, including skin, and inputted into the calibration function to determine the image-based volumetric fractions of the three contents (water, lipid, and protein)

$$f_i = a_0 + a_1 U^L + a_2 U^H. \quad (2)$$

2.D. Spectral distortion correction

Current CZT-based photon-counting detectors suffer discernible spectral distortions, due to limited counting capability, pulse pileup, charge-sharing, and other artifacts.[49,54–56] The benefits of photon-counting detectors in material identification can be substantially deteriorated with the presence of such spectral distortions, especially for the investigated three-material decomposition where the x-ray attenuation difference of the three components are very small. In current study, we initially investigated the accuracy of dual energy decomposition based on raw images, which utilized all detected photons. Then we investigated the feasibility of dual energy tissue decomposition with two correction methods. In the first method, which will be referred to as the energy-cropped method, an energy threshold at 90 keV was used to reject all counts above this energy for the 100 kV(peak) beam (see Fig. 2). Dual energy decomposition was performed only with photons whose energy was below 90 keV. The rejection of the high energy counts clearly led to dose penalty for clinical imaging. However, it helps to exclude pulse pileup effect due to limited counting capability.

In the second method, which will be referred to as spectral-corrected method, an image-based correction on the raw images in the projection domain was used. Dual energy decomposition was then carried out with spectral-corrected images, which utilized all available photons. In this method, the photon counts in the ith energy bin were measured experimentally (N_i^{exp}) at various calibration thicknesses since this correction is flux dependent. At the same time, the expected counts in ith energy bin at the corresponding calibration thickness were simulated (N_i^{sim}) for an ideal detector without any image and spectral artifacts using a previously reported technique based on a tungsten anode spectral model using interpolating polynomials (TASMIP).[57] Thus, the relationship between N_i^{exp} and N_i^{sim} was fitted with an empirical fitting function from the recent report[58]

$$N_i^{\text{sim}} = \frac{x_0 + x_1 N_i^{\text{exp}}}{1 + x_2 N_i^{\text{exp}}}. \quad (3)$$

Three fitting parameters (x_0, x_1, and x_2) were introduced to accommodate for the nonlinear relations between the simulated and the measured counts. This correction procedure was repeated in each energy bin with five sets of fitting parameters being obtained separately. This was applied to the raw images in the corresponding energy bin for the spectral distortion correction. This method corrected all distortions induced by pulse pileup, charge-sharing, and other artifacts and were shown to be successful in a phantom study.[50]

2.E. Chemical analysis

The tissue composition measured from chemical decomposition was used as the gold standard to justify the feasibility of the proposed dual energy decomposition technique and to compare the accuracy of three approaches in image processing. The chemical analysis method was based on a standardized procedure devised by the United States Department of Agriculture to measure the content of water, lipid, lean, and mineral in a sample.[59] Each postmortem breast was weighed before and after placing them in a 95° oven for at least 48 h to get the mass of pure water. Next, the sample was grounded into slurry and mixed with petroleum ether, and then filtered using a Buchner funnel to extract the mass of protein. Finally, the petroleum ether was evaporated using heat and vacuum distillation to isolate the lipid content and determine the lipid mass.[60] Skin was also included in the chemical analysis, so that the total volume under investigation was consistent with the image-based measurement. The measured masses of water, lipid, and protein content were converted into volumes through the known densities, respectively. The error from chemical analysis was estimated to be approximately 1%.[61,62]

3. RESULTS

The volumetric fractions of water, lipid, and protein content in the postmortem breasts were measured using dual energy decomposition and compared to the gold standard obtained from chemical analysis. The results from the raw and the energy-cropped images are presented in Fig. 3, where the volumetric fractions of water, lipid, and protein content are plotted as a function of those from chemical analysis. Linear regression analysis was performed for each component, and is shown as the dashed line in the plot. The tissue compositional measurement from chemical analysis agreed well with the report in literature.[16,63] The volumetric fractions of water and lipid content were measured with a wide range, due to large variations in breast density among all postmortem breasts. Protein content was generally measured to be less than 10%. It should also be noted that the fraction of lipid is inversely

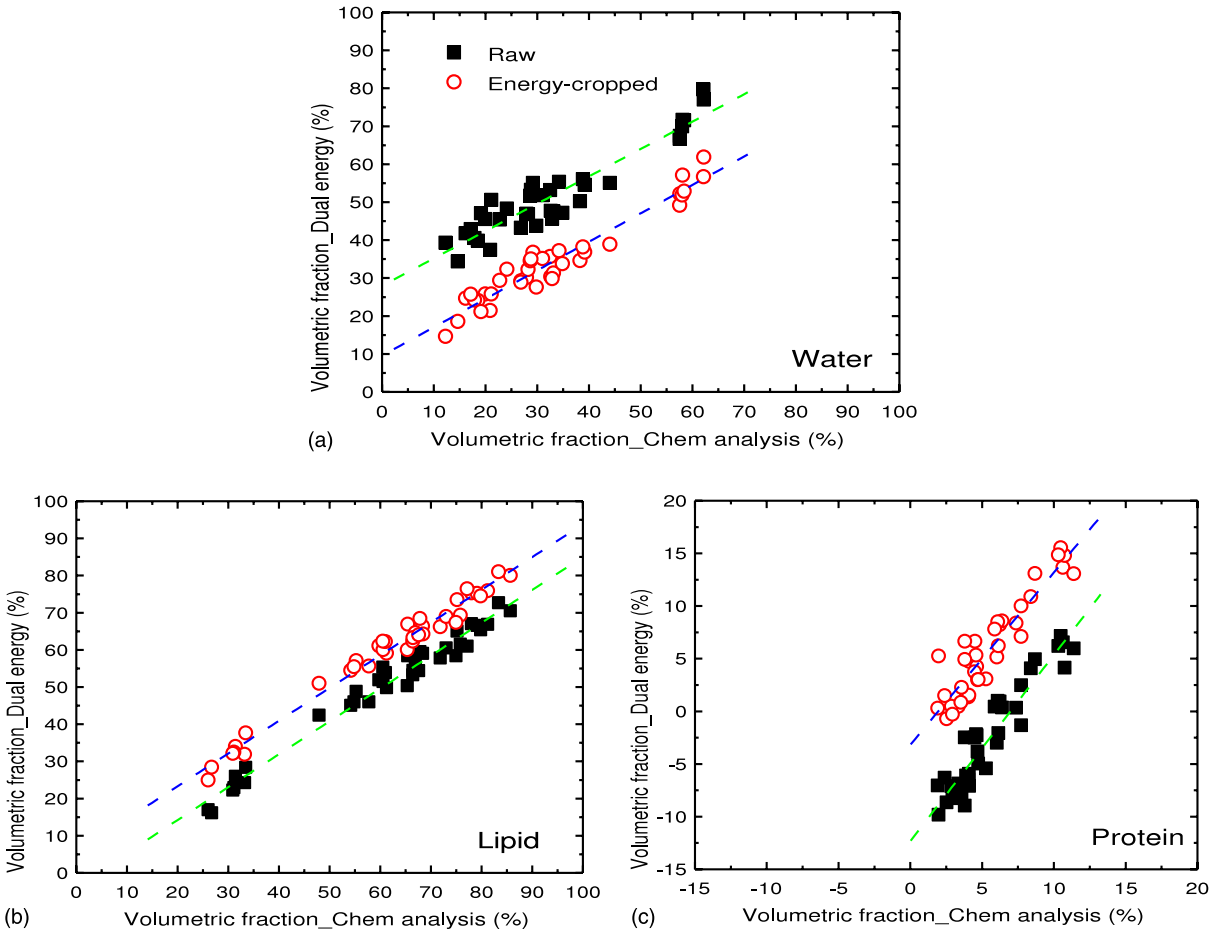

FIG. 3. Correlations of the volumetric fractions of water (a), lipid (b), and protein (c) content derived from dual energy imaging and chemical analysis. Shown in solid squares and hollow circles, respectively, is the dual energy decomposition using the raw images, which suffered from spectral distortions, and the energy-cropped images, which only utilized photons below 90 keV. The correlations were fitted by straight lines for each type of image. Please note that figure (c) is presented in a different scale from (a) and (b) due to the small fraction of protein in breast tissue.

correlated to that of water for a given breast since the two contents were found primarily in adipose and glandular tissues, respectively. On the other hand, protein fraction correlated to water positively, as it can only be found in the glandular tissue. The volumetric fractions of the three components obtained from dual energy decomposition have good linear correlations with respect to those from chemical analysis for both raw and energy-cropped images. The Pearson's correlation coefficient r, derived from linear regression, was estimated to be larger than 0.9 in all cases (Table I). In particular, the linear correlation was slightly improved for water content when the energy-cropped images were used for dual energy decomposition. The slopes of the linear fittings were almost identical for the raw and the energy-cropped images. However, large differences were observed in the intercept values for the two types of images. When performing dual energy decomposition directly on the raw images, a large intercept value was observed for water content, which suggested a systematic error in the quantitative characterization of the breast tissue. In addition, negative fractions were obtained for protein content in some breasts due to the presence of spectral distortion in the raw images. Using energy-cropped images,

TABLE I. Summary of the linear regression analysis of tissue decomposition results from dual energy imaging using the raw, energy-cropped, and spectral-corrected images.

	Water			Lipid			Protein		
	Raw	Energy-cropped	Spectral-corrected	Raw	Energy-cropped	Spectral-corrected	Raw	Energy-cropped	Spectral-corrected
Slope	0.72	0.75	0.99	0.88	0.88	0.97	1.77	1.64	0.88
Intercept	27.98	9.56	−0.24	−3.45	5.71	2.89	−12.33	−3.18	0.43
Pearson's r	0.94	0.97	0.97	0.99	0.99	0.98	0.94	0.92	0.78
RMS error	19.52	4.8	3.5	10.96	3.35	3.27	8.45	2.46	1.89

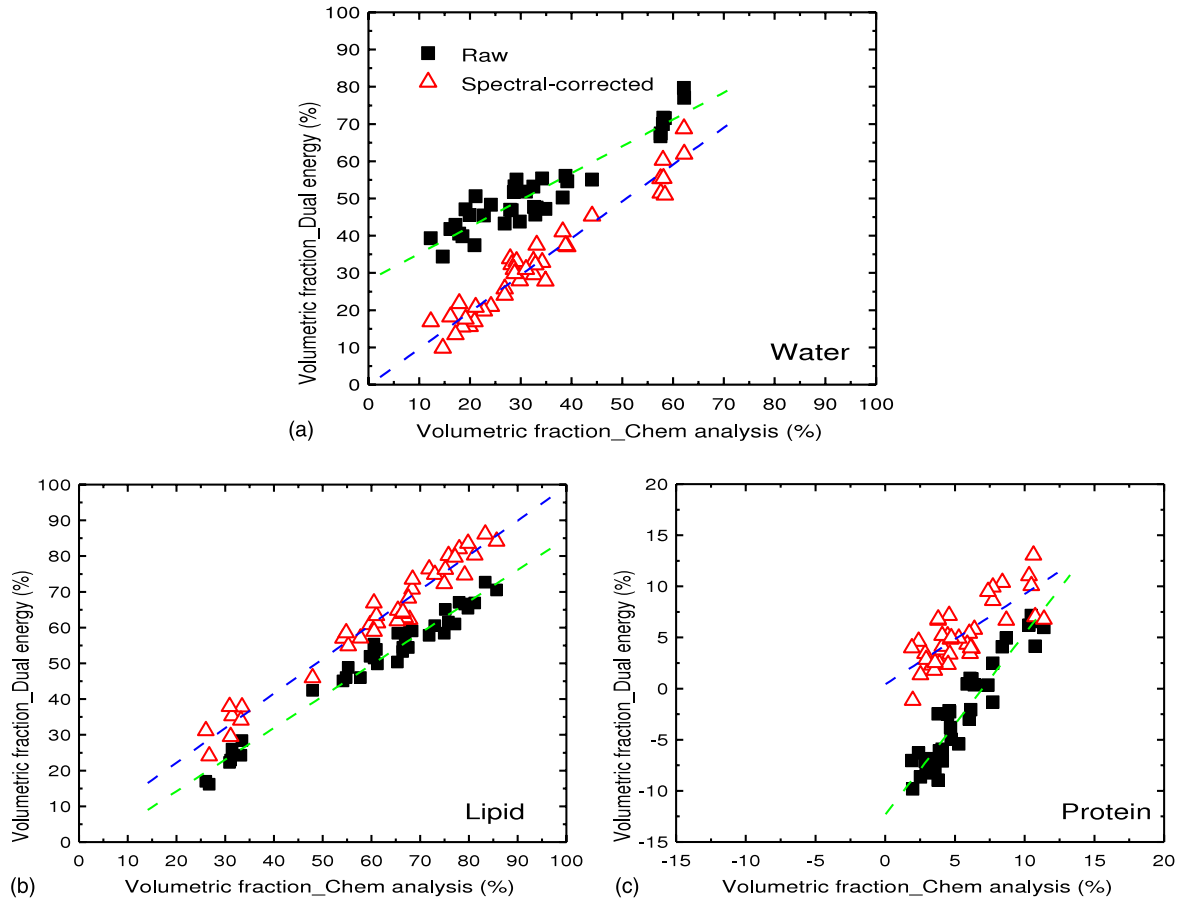

FIG. 4. Correlations of the volumetric fractions of water (a), lipid (b), and protein (c) content derived from dual energy imaging using raw and spectral-corrected images. The range of the plots was kept the same as in Fig. 3 for visual comparison. Linear fittings for all three contents are shown in dashed lines. Please note that Fig. 3(c) is presented in a different scale from (a) and (b) due to the small fraction of protein in breast tissue.

which removed photons above 90 keV, the measured water content was consistently reduced while the lipid and protein content increased for all breasts due to the reduction of pulse pileup artifacts. It can be seen that most protein fractions were above zero in this case.

Dual energy decomposition was also performed on the spectral-corrected images, where all available photons were used in the analysis. The results from the spectral-corrected images, together with the raw images, are shown in Fig. 4. Linear fits were performed and noted by dashed lines in each plot. Excellent correlations can be found for water and lipid content, while Pearson's r was reduced in the case of protein when comparing the raw and energy-cropped images (Table I). However, the decrease in protein correlation can be largely explained by the reduction in data range, and can be attributed to the inherent limitations of linear regression analysis.[64] The most significant improvement with the corrected images can be found in the slopes and the intercept values of the linear fittings, which are now almost identical to the identity lines in the plots for all three components (Table I). The improvement in fitting slope and intercept values led to substantial reduction of the errors in tissue compositional characterization. Using the reference standard from chemical analysis, the root-mean-square (RMS) errors from the dual energy measurements of all breasts are shown in Fig. 5 for water, lipid, and protein content. In the case of water, the RMS error decreased from 19.5% to 4.8% by rejecting some of the high energy photons in the images, and was further reduced to 3.5% when spectral distortion correction technique was used for all available photons. Similar situations can be found in cases of lipid and protein as well, where the errors from the spectral-corrected images were estimated to be 3.3% and 1.9%, respectively.

The accuracy of the dual energy decomposition techniques was also studied for each breast. In this case, the RMS errors in tissue compositional characterizations were derived from the measured fractions of all three components in a given breast and plotted for each of the 38 breasts in Fig. 6. The averaged RMS errors were calculated and indicated by dashed lines in the plot for the three types of images. The sample index was given based on the weighted mass of each breast in an ascending order. As one may expect from the earlier results, the averaged RMS error in tissue characterization was significantly reduced down to 2.8% by applying the spectral distortion correction technique on the raw images. It is also interesting to note that, in the raw image results, the decomposition errors showed a certain degree of correlation with respect to the sample mass, where large breasts generally led to higher errors. This can be attributed to the fact that large breasts lead to more significant

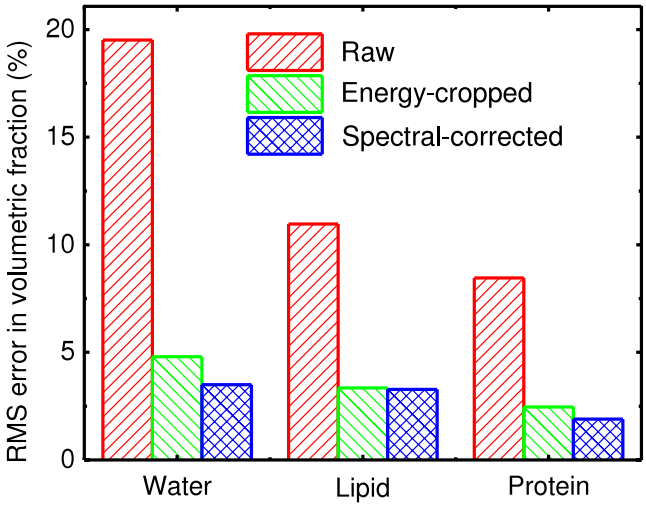

FIG. 5. Comparison of the RMS errors for water, lipid, and protein quantifications with dual energy imaging using the raw, the energy-cropped, and the spectral-corrected images.

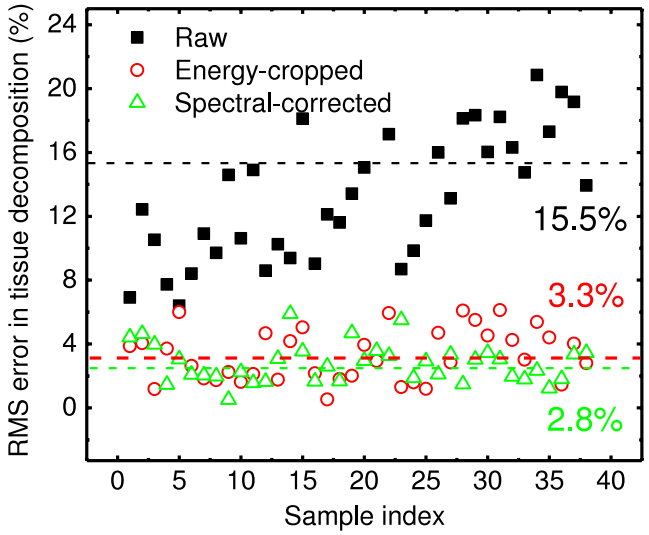

FIG. 6. RMS error in tissue characterization for all 38 postmortem breasts. Sample index was given according to increasing breast mass. The averaged RMS errors are shown as dashed lines for the corresponding imaging processing method, respectively.

flux variations, hence, the attenuation measurement becomes more unreliable with the nonlinear flux-dependent detector response.

4. DISCUSSION

The discrimination capability for suspicious lesions is critical for the improvement of the positive predictive values in breast cancer detection.[17] However, it is extremely challenging to quantify the three primary components (water, lipid, and protein) of a lesion due to the small differences in their x-ray attenuation properties. The current study investigated the feasibility of dual energy tissue compositional characterization using a spectral CT system based on an energy-resolved photon-counting CZT detector. Postmortem breasts were imaged in this study so that the definitive tissue composition, in terms of water, lipid, and protein content, can be derived from chemical analysis. The results from chemical analysis offered a reference standard to assess the accuracy of the proposed dual energy decomposition technique. The results of this study suggested that the chemical composition of breast tissue can be characterized accurately at a dose level of 2 mGy with CZT-based spectral CT after spectral correction of the images. The estimated error from dual energy decomposition was less than 3%. Although the current study used the entire breast volume for the measurement, the proposed technique can be readily implemented to characterize the chemical composition of lesions with small volumes. With a reliable technique for tissue characterization, future studies can then be conducted to investigate the compositional differences between malignant and normal tissues.

Despite the exciting advancement in detector technology, current photon-counting detectors still face great challenges for clinical applications. The high photon flux required in clinical x-ray imaging leads to artifacts that will severely undermine the image quality and the accuracy of quantitative analysis. One of the major issues with the investigated CZT detector is the nonlinear intensity response induced by pulse pileup.[49,50,56,58] Under high flux, multiple photons arriving closer in time than the dead time of the readout electronics will be recorded as a single count and mistakenly registered into the high energy bin. Such behavior effectively increases the spectral overlap between the low and high energy images used for dual energy decomposition. Consequently, for a given breast volume, the reconstructed attenuation coefficient decreases in the low energy image, while increasing in the high energy image. Such nonlinear artifacts cannot be corrected using standard system calibration procedures. Thus, it will lead to unreliable material decomposition as shown in Fig. 6. Another common problem with photon-counting detectors is charge-sharing. However, charge-sharing fraction does not depend on the incident photon flux. Therefore, the errors induced by charge-sharing can be, to a large degree, offset by a system calibration.

Two independent spectral correction methods have been investigated in this study. In the first method, a high energy threshold was used to reject most of the pileup photons. The selection of the cropping energy at 90 keV for the 100 kV(peak) spectrum used in the study was a compromise between image quality and dose penalty. It should also be noted that since the splitting energy was selected at 42 keV, the 90 keV cropping energy basically rejected most of the pileup photons in a high energy image, considering the limited energy resolution of the detector.[65] A preliminary phantom study using bovine tissue has shown that the RMS error in water fraction reduces from 7.2% to 4.9% and 4.0%, when the cropping energy is reduced from 100 to 90 and 80 keV, respectively. Shifting the cropping energy further will not only cause more dose penalty, but also increases the quantum noise, which in turn reduces the accuracy of dual energy decomposition. It should also be noted that this method does not address the possible errors induced by charge-sharing. However, the improvement in accuracy for

dual energy decomposition was quite significant. This finding corroborates the earlier discussions that charge-sharing may not contribute significantly to the errors in the dual energy decomposition.

Despite the advantage of simplicity in implementation, there are several limitations with the first correction method. First, approximately 3%–5% of the photons that have penetrated through the breast are not used in dual energy decomposition. In addition, the pileup photons that originated from the low energy bin cannot be corrected, as their energies fell into the same range as the primary photons for the high energy image. Both issues were addressed with the implementation of the spectral distortion correction method, where all available photons were correctly registered into the low and high energy bins, and the spectral overlap was minimized. The small decomposition error and the consistency among all breasts are indicative of the accuracy of the spectral distortion correction technique.

Current study employed narrow beam geometry with good scatter rejection, which not only improved the accuracy of dual energy decomposition, but also reduced the required dose for a reliable measurement. Comparing to a similar study using a flat-panel-based cone-beam CT system, the RMS error in tissue characterization was reduced from approximately 3.6% to 2.8% using one-third of the dose.[16] For future clinical implementations, an ideal system should employ a multislice multislit geometry for the optimal performance in scatter rejection and dose efficiency. For current cone-beam CT systems, a proper design of the decomposition calibration phantom, which may offset some of the errors induced by scatter, will be critical to minimize the errors in quantitative tissue characterization.[16] The improvement from the implementation of scatter correction algorithms should also be investigated.

5. CONCLUSION

This postmortem study indicated that spectral CT based on an energy-resolved photon-counting detector can be used to accurately characterize the chemical composition of breast tissue in terms of water, lipid, and protein content with a low radiation dose. The dual energy compositional analysis of a lesion can potentially improve the sensitivity and specificity of breast cancer diagnosis.

ACKNOWLEDGMENTS

This work was supported in part by NIH/NCI grant R01CA13687. The authors would like to thank David Rundle from Endicott Interconnect Detection and Imaging Systems for his technical support and fruitful discussions.

[a]Author to whom correspondence should be addressed. Electronic mail: symolloi@uci.edu; Telephone: (949) 824-5904; Fax: (949) 824-8115.

[1]S. Feig, "Comparison of costs and benefits of breast cancer screening with mammography, ultrasonography, and MRI," Obstet. Gynecol. Clin. North Am. **38**, 179–196 (2011).
[2]F. Diekmann, M. Freyer, S. Diekmann, E. M. Fallenberg, T. Fischer, U. Bick, and A. Pollinger, "Evaluation of contrast-enhanced digital mammography," Eur. J. Radiol. **78**, 112–121 (2011).
[3]K. Pinker, N. Perry, S. Milner, K. Mokbel, and S. Duffy, "Accuracy of breast cancer detection with full-field digital mammography and integral computer-aided detection correlated with breast density as assessed by a new automated volumetric breast density measurement system," Breast Cancer Res. **12**, 4 (2010).
[4]*Ibid.*, "Sensitivity of integral computer-aided detection with full-field digital mammography for detection of breast cancer according to different histopathological tumor types and appearances," Breast Cancer Res. **12**, 13 (2010).
[5]B. Chen and R. Ning, "Cone-beam volume CT breast imaging: Feasibility study," Med. Phys. **29**, 755–770 (2002).
[6]R. Ning, D. L. Conover, Y. Yu, Y. Zhang, S. Liu, and J. Neugebauer, "Koning cone beam breast CT for breast cancer detection, diagnosis and treatment," Am. J. Clin. Oncol.-Cancer Clin. Trials **33**, 526–527 (2010).
[7]J. M. Boone and T. R. Nelson, "The case for dedicated CT screening for breast cancer," Radiology **217**, 346 (2000).
[8]J. M. Boone, T. R. Nelson, K. K. Lindfors, and J. A. Seibert, "Dedicated breast CT: Radiation dose and image quality evaluation," Radiology **221**, 657–667 (2001).
[9]K. K. Lindfors, J. M. Boone, T. R. Nelson, K. Yang, A. L. C. Kwan, and D. F. Miller, "Dedicated breast CT: Initial clinical experience," Radiology **246**, 725–733 (2008).
[10]M. Tomai, P. Madhav, D. Crotty, S. Cutler, K. Perez, R. McKinley, and J. Bowsher, "Application of volumetric molecular breast imaging with a dedicated SPECT-CT mammotomograph," Med. Phys. **34**, 2597 (2007).
[11]M. P. Tornai and R. L. McKinley, "A high-performance SPECT-CT system for dedicated molecular breast imaging," J. Nucl. Med. **52**, 673–674 (2011).
[12]L. Y. Chen, Y. T. Shen, C. J. Lai, T. Han, Y. C. Zhong, S. A. P. Ge, X. M. Liu, T. P. Wang, W. T. Yang, G. J. Whitman, and C. C. Shaw, "Dual resolution cone beam breast CT: A feasibility study," Med. Phys. **36**, 4007–4014 (2009).
[13]W. T. Yang, C. C. Shaw, L. Chen, C. Altunbas, T. Wang, C. J. Lai, K. Cheenu, S. J. Tu, X. Liu, and G. J. Whitman, "Cone beam breast CT—A feasibility study with surgical mastectomy specimens," Breast Cancer Res. Treat. **94**, S210 (2005).
[14]S. J. Glick, "Breast CT," Annu. Rev. Biomed. Eng. **9**, 501–526 (2007).
[15]H. Ding, J. L. Ducote, and S. Molloi, "Breast composition measurement with a cadmium-zinc-telluride based spectral computed tomography system," Med. Phys. **39**, 1289–1297 (2012).
[16]H. Ding, J. L. Ducote, and S. Molloi, "Measurement of breast tissue composition with dual energy cone-beam computed tomography: A postmortem study," Med. Phys. **40**, 061902 (9pp.) (2013).
[17]R. W. Woods, G. S. Sisney, L. R. Salkowski, K. Shinki, Y. Lin, and E. S. Burnside, "The mammographic density of a mass is a significant predictor of breast cancer," Radiology **258**, 417–425 (2011).
[18]G. McIntyre, "Increased cell hydration promotes both tumor growth and metastasis: A biochemical mechanism consistent with genetic signatures," Med. Hypotheses **69**, 1127–1130 (2007).
[19]S. Chung, A. Cerussi, C. Klifa, H. Baek, O. Birgul, G. Gulsen, S. Merritt, D. Hsiang, and B. Tromberg, "In vivo water state measurements in breast cancer using broadband diffuse optical spectroscopy," Phys. Med. Biol. **53**, 6713–6727 (2008).
[20]D. Hsiang, A. Durkin, J. Butler, B. J. Tromberg, A. Cerussi, and N. Shah, "In vivo absorption, scattering, and physiologic properties of 58 malignant breast tumors determined by broadband diffuse optical spectroscopy," J. Biomed. Opt. **11**, 044005 (2006).
[21]B. J. Tromberg, A. Cerussi, N. Shah, M. Compton, A. Durkin, D. Hsiang, J. Butler, and R. Mehta, "Imaging in breast cancer: Diffuse optics in breast cancer: Detecting tumors in pre-menopausal women and monitoring neoadjuvant chemotherapy," Breast Cancer Res. **7**, 279–285 (2005).
[22]A. S. Haka, K. E. Shafer-Peltier, M. Fitzmaurice, J. Crowe, R. R. Dasari, and M. S. Feld, "Diagnosing breast cancer by using Raman spectroscopy," Proc. Natl. Acad. Sci. U. S. A. **102**, 12371–12376 (2005).
[23]E. G. Olmstead, *Mammalian Cell Water; Physiologic and Clinical Aspects* (American College of Physicians, Philadelphia, PA, 1966).
[24]L. W. Sha, E. R. Ward, and B. Stroy, "A review of dielectric properties of normal and malignant breast tissue," in *IEEE Southeastcon 2002: Proceedings* (IEEE, New York, NY, 2002), pp. 457–462.
[25]K. Drukker, F. Duewer, M. L. Giger, S. Malkov, C. I. Flowers, B. Joe, K. Kerlikowske, J. S. Drukteinis, H. Li, and J. A. Shepherd, "Mammographic

quantitative image analysis and biologic image composition for breast lesion characterization and classification," Med. Phys. **41**, 031915 (8pp.) (2014).
[26]A. D. Laidevant, S. Malkov, C. I. Flowers, K. Kerlikowske, and J. A. Shepherd, "Compositional breast imaging using a dual-energy mammography protocol," Med. Phys. **37**, 164–174 (2010).
[27]E. Roessl and R. Proksa, "K-edge imaging in x-ray computed tomography using multi-bin photon counting detectors," Phys. Med. Biol. **52**, 4679–4696 (2007).
[28]W. A. Kalender, M. Beister, J. M. Boone, D. Kolditz, S. V. Vollmar, and M. C. C. Weigel, "High-resolution spiral CT of the breast at very low dose: Concept and feasibility considerations," Eur. Radiol. **22**, 1–8 (2012).
[29]P. M. Shikhaliev and S. G. Fritz, "Photon counting spectral CT versus conventional CT: Comparative evaluation for breast imaging application," Phys. Med. Biol. **56**, 1905–1930 (2011).
[30]C. Bert, D. Niederlohner, J. Giersch, K. F. Pfeiffer, and G. Anton, "Computed tomography using the Medipix1 chip," Nucl. Instrum. Methods Phys. Res., Sect. A **509**, 240–250 (2003).
[31]M. G. Bisogni, A. Del Guerra, N. Lanconelli, A. Lauria, G. Mettivier, M. C. Montesi, D. Panetta, R. Pani, M. G. Quattrocchi, P. Randaccio, V. Rosso, and P. Russo, "Experimental study of beam hardening artifacts in photon counting breast computed tomography," Nucl. Instrum. Methods Phys. Res., Sect. A **581**, 94–98 (2007).
[32]M. Chmeissani, C. Frojdh, O. Gal, X. Llopart, J. Ludwig, M. Maiorino, E. Manach, G. Mettivier, M. C. Montesi, C. Ponchut, P. Russo, L. Tlustos, and A. Zwerger, "First experimental tests with a CdTe photon counting pixel detector hybridized with a Medipix2 readout chip," IEEE Trans. Nucl. Sci. **51**, 2379–2385 (2004).
[33]P. M. Frallicciardi, J. Jakubek, D. Vavrik, and J. Dammer, "Comparison of single-photon counting and charge-integrating detectors for x-ray high-resolution imaging of small biological objects," Nucl. Instrum. Methods Phys. Res., Sect. A **607**, 221–222 (2009).
[34]D. Niederlohner, F. Nachtrab, T. Michel, and G. Anton, "Using the Medipix2 detector for photon counting computed tomography," *Presented at the Nuclear Science Symposium Conference Record*, IEEE, Fajardo, Puerto Rico, October 23–29 (2005).
[35]D. J. Wagenaar, S. Chowdhury, J. C. Engdahl, and D. D. Burckhardt, "Planar image quality comparison between a CdZnTe prototype and a standard NaI(T1) gamma camera," Nucl. Instrum. Methods Phys. Res., Sect. A **505**, 586–589 (2003).
[36]X. Wang, D. Meier, S. Mikkelsen, G. E. Maehlum, D. J. Wagenaar, B. M. W. Tsui, B. E. Patt, and E. C. Frey, "MicroCT with energy-resolved photon-counting detectors," Phys. Med. Biol. **56**, 2791–2816 (2011).
[37]W. C. Barber, E. Nygard, J. S. Iwanczyk, M. Zhang, E. C. Frey, B. Tsui, J. C. Wessel, N. Malakhov, G. Wawrzyniak, N. E. Hartsough, T. Gandhi, and K. Taguchi, "Characterization of a novel photon counting detector for clinical CT: Count rate, energy resolution, and noise performance," Proc. SPIE **7258**, 725824 (2009).
[38]D. Pan, E. Roessl, J. P. Schlomka, S. D. Caruthers, A. Senpan, M. J. Scott, J. S. Allen, H. Y. Zhang, G. Hu, P. J. Gaffney, E. T. Choi, V. Rasche, S. A. Wickline, R. Proksa, and G. M. Lanza, "Computed tomography in color: NanoK-enhanced spectral CT molecular imaging," Angew. Chem. Int., Ed. **49**, 9635–9639 (2010).
[39]H. Toyokawa, Y. Furukawa, T. Hirono, H. Ikeda, K. Kajiwara, M. Kawase, T. Ohata, G. Sato, M. Sato, T. Takahashi, H. Tanida, T. Uruga, and S. Watanabe, "Si and CdTe pixel detector developments at SPring-8," Nucl. Instrum. Methods Phys. Res., Sect. A **636**, S218–S221 (2011).
[40]T. Takahashi and S. Watanabe, "Recent progress in CdTe and CdZnTe detectors," IEEE Trans. Nucl. Sci. **48**, 950–959 (2001).
[41]H. Q. Le and S. Molloi, "Segmentation and quantification of materials with energy discriminating computed tomography: A phantom study," Med. Phys. **38**, 228–237 (2011).
[42]M. Prokesch, D. S. Bale, and C. Szeles, "Fast high-flux response of CdZnTe x-ray detectors by optical manipulation of deep level defect occupations," IEEE Trans. Nucl. Sci. **57**, 2397–2399 (2010).
[43]W. C. Barber, E. Nygard, J. C. Wessel, N. Malakhov, G. Wawrzyniak, N. E. Hartsough, T. Gandhi, and J. S. Iwanczyk, "Fast photon counting CdTe detectors for diagnostic clinical CT: Dynamic range, stability, and temporal response," Proc. SPIE **7622**, 76221E (2010).
[44]D. Greiffenberg, A. Cecilia, A. Zwerger, A. Fauler, P. Vagovic, J. Butzer, E. Hamann, T. dos Santos Rolo, T. Baumbach, and M. Fiederle, "Investigations of the high flux behavior of CdTe-Medipix2 assemblies at the synchrotron ANKA," *Presented at the Nuclear Science Symposium Conference Record (NSS/MIC)*, Knoxville, TN, October 30–November 6 (2010).
[45]S. Miyajima, "Thin CdTe detector in diagnostic x-ray spectroscopy," Med. Phys. **30**, 771–777 (2003).
[46]S. Miyajima, K. Imagawa, and M. Matsumoto, "CdZnTe detector in diagnostic x-ray spectroscopy," Med. Phys. **29**, 1421–1429 (2002).
[47]S. G. Fritz, P. M. Shikhaliev, and K. L. Matthews, "Improved x-ray spectroscopy with room temperature CZT detectors," Phys. Med. Biol. **56**, 5735–5751 (2011).
[48]U. Bottigli, B. Golosio, G. L. Masala, P. Oliva, S. Stumbo, P. Delogu, M. E. Fantacci, L. Abbene, F. Fauci, and G. Raso, "Comparison of two portable solid state detectors with an improved collimation and alignment device for mammographic x-ray spectroscopy," Med. Phys. **33**, 3469–3477 (2006).
[49]A. S. Wang, D. Harrison, V. Lobastov, and J. E. Tkaczyk, "Pulse pileup statistics for energy discriminating photon counting x-ray detectors," Med. Phys. **38**, 4265–4275 (2011).
[50]H. Ding and S. Molloi, "Image-based spectral distortion correction for photon-counting x-ray detectors," Med. Phys. **39**, 1864–1876 (2012).
[51]J. P. Wilson, K. Mulligan, B. Fan, J. L. Sherman, E. J. Murphy, V. W. Tai, C. L. Powers, L. Marquez, V. Ruiz-Barros, and J. A. Shepherd, "Dual-energy x-ray absorptiometry-based body volume measurement for 4-compartment body composition," Am. J. Clin. Nutr. **95**, 25–31 (2012).
[52]J. M. Boone, "Normalized glandular dose (DgN) coefficients for arbitrary x-ray spectra in mammography: Computer-fit values of Monte Carlo derived data," Med. Phys. **29**, 869–875 (2002).
[53]J. B. Sheffield, "ImageJ, a useful tool for biological image processing and analysis," Microsc. Microanal. **13**, 200–201 (2007).
[54]C. Xu, M. Danielsson, and H. Bornefalk, "Evaluation of energy loss and charge sharing in cadmium telluride detectors for photon-counting computed tomography," IEEE Trans. Nucl. Sci. **58**, 614–625 (2011).
[55]K. Taguchi, M. Zhang, E. C. Frey, X. Wang, J. S. Iwanczyk, E. Nygard, N. E. Hartsough, B. M. W. Tsui, and W. C. Barber, "Modeling the performance of a photon counting x-ray detector for CT: Energy response and pulse pileup effects," Med. Phys. **38**, 1089–1102 (2011).
[56]M. Strassburg, C. Schroeter, and P. Hackenschmied, "CdTe/CZT under high flux irradiation," J. Instrum. **6**, C01055 (2011).
[57]J. M. Boone and J. A. Seibert, "Accurate method for computer-generating tungsten anode x-ray spectra from 30 to 140 kV," Med. Phys. **24**, 1661–1670 (1997).
[58]K. Taguchi, E. C. Frey, X. L. Wang, J. S. Iwanczyk, and W. C. Barber, "An analytical model of the effects of pulse pileup on the energy spectrum recorded by energy resolved photon counting x-ray detectors," Med. Phys. **37**, 3957–3969 (2010).
[59]*Determination of Fat CLG-FAT* (Food Safety and Inspection Service, Office of Public Health Science, Washington, DC, 2009).
[60]B. Zhao, H. Gao, H. Ding, and S. Molloi, "Tight-frame based iterative image reconstruction for spectral breast CT," Med. Phys. **40**, 031905 (10pp.) (2013).
[61]J. L. Ducote, M. J. Klopfer, and S. Molloi, "Volumetric lean percentage measurement using dual energy mammography," Med. Phys. **38**, 4498–4504 (2011).
[62]T. Johnson, H. Ding, H. Q. Le, J. L. Ducote, and S. Molloi, "Breast density quantification with cone-beam CT: A post-mortem study," Phys. Med. Biol. **58**, 8573–8591 (2013).
[63]H. Q. Woodard and D. R. White, "The composition of body tissues," Br. J. Radiol. **59**, 1209–1218 (1986).
[64]J. M. Bland and D. G. Altman, "Statistical methods for assessing agreement between two methods of clinical measurement," Lancet **1**, 307–310 (1986).
[65]C. Szeles, S. A. Soldner, S. Vydrin, J. Graves, and D. S. Bale, "CdZnTe semiconductor detectors for spectroscopic x-ray imaging," IEEE Trans. Nucl. Sci. **55**, 572–582 (2008).